Am J Physiol Renal Physiol 318: F388–F401, 2020.
First published December 16, 2019; doi:10.1152/ajprenal.00419.2019.

RESEARCH ARTICLE

Effects of a prolyl hydroxylase inhibitor on kidney and cardiovascular complications in a rat model of chronic kidney disease

Lisa Uchida,[1] Tetsuhiro Tanaka,[1] Hisako Saito,[1] Mai Sugahara,[1] Takeshi Wakashima,[1,2] Kenji Fukui,[1,2] and Masaomi Nangaku[1]

[1]*Division of Nephrology and Endocrinology, the University of Tokyo Graduate School of Medicine, Tokyo, Japan; and* [2]*Biological and Pharmacological Research Laboratories, Central Pharmaceutical Research Institute, Japan Tobacco Incorporated, Takatsuki, Japan*

Submitted 6 September 2019; accepted in final form 10 December 2019

Uchida L, Tanaka T, Saito H, Sugahara M, Wakashima T, Fukui K, Nangaku M. Effects of a prolyl hydroxylase inhibitor on kidney and cardiovascular complications in a rat model of chronic kidney disease. *Am J Physiol Renal Physiol* 318: F388–F401, 2020. First published December 16, 2019; doi:10.1152/ajprenal.00419.2019.—Cardiovascular disease (CVD) is the main cause of death in patients with kidney disease. Hypoxia plays a crucial role in the progression of chronic kidney disease (CKD) and cardiovascular disease, which is associated with fibrosis, inflammation, and oxidative injury. Previous studies have indicated that prolyl hydroxylase (PHD) inhibitors, stabilizers of hypoxia-inducible factors (HIFs), can be used to treat acute organ injuries such as renal ischemia-reperfusion, myocardial infarction, and, in some contexts, CKD. However, the effects of PHD inhibitors on cardiovascular complications in CKD remain unknown. In the present study, we investigated whether HIF activation has a beneficial effect on kidney and cardiovascular outcomes in the remnant kidney model. We used the 5/6 nephrectomy model with the nitric oxide synthase inhibitor N^{ω}-nitro-L-arginine (20 mg/L in the drinking water). Rats received diet with 0.005% enarodustat (PHD inhibitor) or vehicle for 8 wk starting 2 wk before 5/6 nephrectomy. Activation of HIF by the PHD inhibitor reduced cardiac hypertrophy and ameliorated myocardial fibrosis in association with restored capillary density and improvement in mitochondrial morphology. With regard to kidneys, enarodustat ameliorated fibrosis in association with reduced proinflammatory cytokine expression, reduced apoptosis, and restored capillary density, even though renal endpoints such as proteinuria and serum creatinine levels were not significantly affected by enarodustat, except for blood urea nitrogen levels at 4 wk. In addition, cardiac hypertrophy marker genes, including atrial natriuretic peptide, were suppressed in P19CL6 cells treated with enarodustat. These findings suggest that PHD inhibitors might show beneficial effects in cardiovascular complications caused by CKD.

cardiorenal syndrome; cardiovascular disease; chronic kidney disease; hypoxia-inducible factor; prolyl hydroxylase inhibitor

INTRODUCTION

Cardiovascular disease (CVD) is the leading cause of death in patients with chronic kidney disease (CKD). There has been increasing recognition that many patients with CKD die of heart disease before they reach end-stage renal disease (see Ref. 11). Interactions between the heart and kidneys are bidirectional, and dysfunction in one organ influences the other; this complex phenomenon is referred to as cardiorenal syndrome (see Ref. 31). Although the mechanisms underlying CVD progression in patients with CKD have yet to be fully elucidated, hemodynamic and fluid status, neurohormonal responses, and CVD-related mechanisms are major contributors to the progression of cardiorenal syndrome (35).

Left ventricular hypertrophy (LVH) is found in ~60–80% of patients starting renal replacement therapy, and the left ventricular mass index increases even in early stage CKD (3, 4, 20). Furthermore, LVH is an independent predictor of arrhythmias and sudden death (22). Treatment of LVH is crucial in this population.

Hypoxia is commonly associated with CKD and CVD pathogenesis (24, 37). Hypoxia-inducible factor (HIF) is a key transcription factor that allows cells to adapt to hypoxia and regulates the expression of 100–200 genes, including erythropoietin (EPO) and VEGF (see Ref. 38). With regard to cardiorenal syndrome, indoxyl sulfate, a uremic toxin, impairs the HIF-mediated cellular response in a CKD milieu, which is relevant to the pathogenesis of cardiovascular complications (47). Because of the role of HIF in EPO production, prolyl hydroxylase (PHD) inhibitors that stabilize HIF have been developed to treat anemia in CKD and are expected to be next-generation erythropoiesis-stimulating agents (43). Furthermore, potential impacts of HIF stabilization have been found in multiple pathophysiological conditions other than renal anemia, which include ischemia-reperfusion injury (5, 15, 18), myocardial infarction (16, 19, 25, 50), stroke (9), and critical limb ischemia (27).

Although protective effects of PHD inhibition have been shown in some models of CKD (41, 46, 53), it remains uncertain whether PHD inhibition leads to cardioprotection in the context of CKD. Therefore, we chose a failing heart model using 5/6 nephrectomy with the nitric oxide (NO) synthase inhibitor N^{ω}-nitro-L-arginine (L-NNA). Systolic dysfunction occurred after 8 wk of exposure to L-NNA on a high-salt diet in the remnant kidney model, and LVH occurred 6 wk after 5/6 nephrectomy (7, 40). Therefore, our experimental period continued to 6 wk after the 5/6 nephrectomy in view of the development of LVH and CKD.

Inflammation, apoptosis, and mitochondrial dysfunction are known to accompany both CVD and CKD. The aim of the present study was to assess whether these factors contribute to

Address for reprint requests and other correspondence: M. Nangaku, Div. of Nephrology and Endocrinology, The Univ. of Tokyo Graduate School of Medicine, 7-3-1 Hongo, Bunkyo-ku, Tokyo 113-8655, Japan (e–mail: mnangaku-tky@umin.ac.jp).

the cardiovascular complications and progression of CKD. In addition, the effects of enarodustat on hypertrophic responses to ANG II were investigated in vitro in mouse P19CL6 cells.

MATERIALS AND METHODS

Animal experiments. Sprague-Dawley rats (male, 8 wk old) weighing 250–280 g were allocated to one of three groups as follows: *1*) sham-operated rats with normal diet ($n = 9$), *2*) rats that underwent 5/6 nephrectomy [remnant kidney (RK)] with vehicle-mixed diet ($n = 18$), and *3*) RK rats with 0.005% enarodustat (1, 2, 26)-mixed diet ($n = 14$) [the number of heart samples we acquired for mRNA analyses, electron microscopy analyses, and immunofluorescence experiments was $n = 4$ (1), 10 (2), and 5 (3), respectively] (Fig. 1). 5/6 nephrectomy was conducted by ligation of the upper and lower thirds of the left renal artery followed by right kidney nephrectomy 1 wk later. To accelerate CKD and cardiac changes, L-NNA (20 mg/L, Cayman Chemical, Ann Arbor, MI) was supplemented to drinking water (7). Blood was obtained from the tail vein, and blood urea nitrogen (BUN) and creatinine levels were measured using a commercial kit (Wako, Osaka, Japan). Rats were housed in metabolic cages for 24 h to collect urine. Urinary protein excretion was measured by Bio-Rad assay reagent. Urinary Na^+ and K^+ concentrations were measured using a JCA-BM6010 automated chemistry analyzer (JEOL, Tokyo, Japan). Systolic blood pressure (SBP) was measured using a tail-cuff system (BP-98A, Softron, Yokohama, Japan). At 6 wk, transthoracic echocardiography was performed under anesthesia with xylazine (6.6 mg/kg, MP Biomedicals, Irvine, CA) and pentobarbital sodium [3 mL/kg (10-fold dilution), Kyoritsu Seiyaku, Tokyo, Japan] by intraperitoneal injection, and rats were killed. All animal experiments were approved by the ethics committee of the Graduate School of Medicine, the University of Tokyo (P16–061, H16–263), and performed in accordance with the guidelines established by the committee.

Hematocrit measurement. Blood was collected in glass capillary tubes and centrifuged at 12,000 rpm for 6 min. The percentage by volume of red blood cells was determined using a hematocrit chart.

Echocardiography. Transthoracic echocardiography was performed at 6 wk using a echocardiographic system (Toshiba Xario; Canon Medical Systems, Tochigi, Japan) under anesthesia. Heart rate, interventricular septum thickness (IVSTd), left ventricular posterior wall thickness (LVPWTd), left ventricular internal diameter at diastole (LVIDd) and systole (LVIDs), and fractional shortening (FS) were determined by M-mode echocardiography.

Histology and immunohistochemistry. Masson trichrome and Sirius red staining were used to assess fibrosis. Periodic acid-Schiff staining was used for the semiquantitative scoring of glomerular sclerosis and tubulointerstitial injury, as previously reported (46). Glomerular sclerosis was graded per glomerulus as follows: *0*, no sclerosis; *1*, <25%; *2*, <50%; *3*, <75%; and *4*, ≥75% involved. At least 20 glomeruli were quantified under ×400 magnification and averaged. Tubulointerstitial injury score was determined based on the proportion of tubule dilatations, the distortion of the tubular basement membranes, and atrophy as follows: *0*, none; *1*, <10%; *2*, <25%; *3*, <50%; *4*, <75%; and *5*, ≥75%. More than 20 consecutive fields were examined under ×400 magnification, and the results were averaged. Immunostaining was performed on formalin-fixed or methyl carnoy's-fixed paraffin-embedded sections (3 μm). We used mouse anti-macrophage monoclonal antibody (ED1, Merck Millipore, Billerica, MA), mouse anti-aminopeptidase P monoclonal antibody (JG12, Bender MedSystems, San Bruno, CA), and rabbit anti-HIF-1α antibody (Cayman Chemical, Ann Arbor, MI) as primary antibodies. Color was developed with diaminobenzidine (Wako) and hydrogen peroxide. To measure the myocyte cross-sectional area, frozen sections of the left ventricle (6 μm) were fixed with 4% paraformaldehyde and stained with wheat germ agglutinin (WGA)-Alexa Fluor 488 conjugate (Invitrogen). A fluorescence microscope (BZ-9000, Keyence, Osaka, Japan) was used for evaluation.

Electron microscopy. Left ventricular tissues were fixed in 2.5% glutaraldehyde, 0.1 M phosphate buffer, and 4% paraformaldehyde. The heart block was examined at various magnifications (×5,000, ×10,000, and ×30,000) in five randomly chosen fields using an electron microscope (JEM-1011, JEOL, Tokyo, Japan). The areas of >80–150

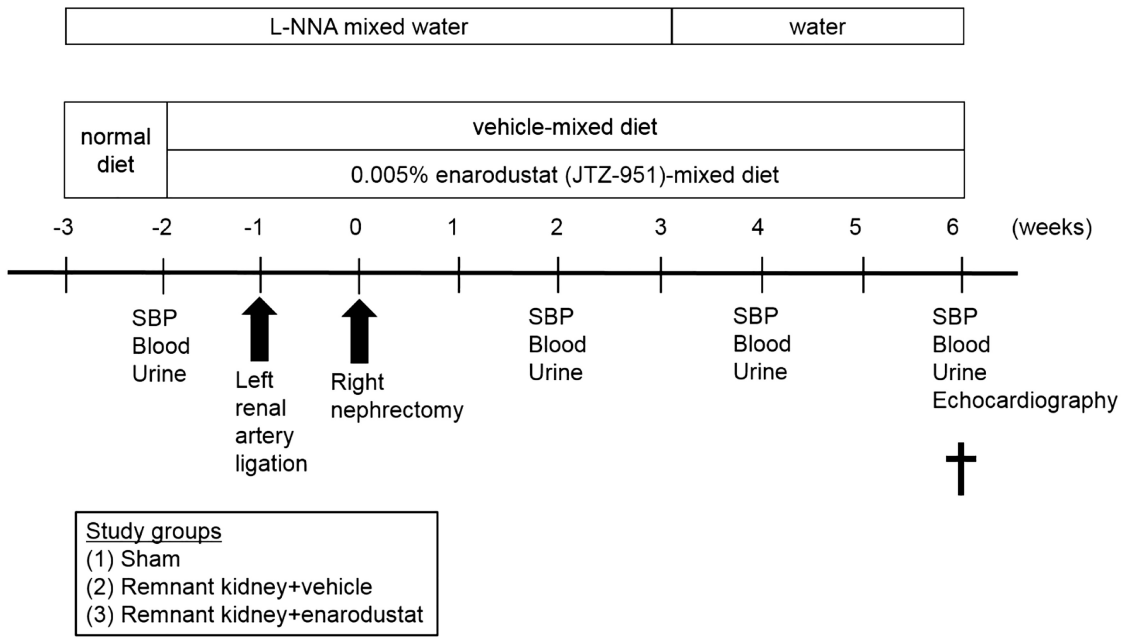

Fig. 1. Protocol of the animal experiment. Male Sprague-Dawley rats (8 wk old) underwent 5/6 nephrectomy [remnant kidney (RK)]. Rats were divided into the following three groups: *1*) sham-operated rats ($n = 9$), *2*) RK rats with a vehicle-mixed diet ($n = 18$), and *3*) RK rats with a 0.005% enarodustat (prolyl hydroxylase inhibitor)-mixed diet ($n = 14$). N^{ω}-nitro-L-arginine (L-NNA; 20 mg/L), a nitric oxide synthase inhibitor, was supplemented in drinking water to accelerate chronic kidney disease and cardiac changes. Systolic blood pressure, blood urea nitrogen, and creatinine levels were measured, and urine samples were collected at −2, 2, 4, and 6 wk. At 6 wk, the kidneys and hearts were harvested after the echocardiography.

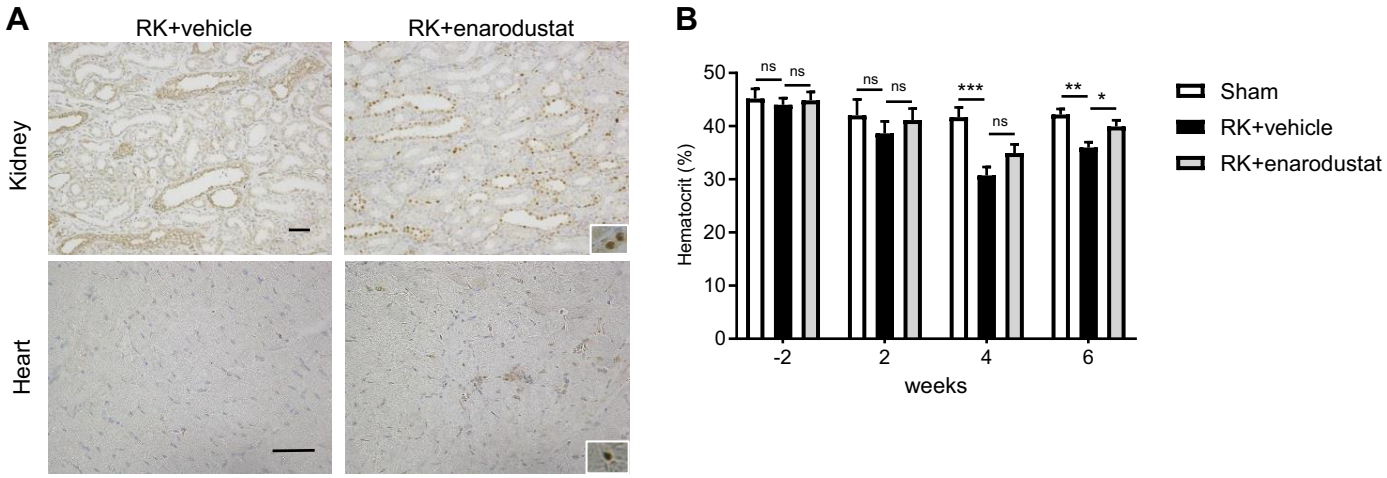

Fig. 2. Hypoxia-inducible factor (HIF) stabilization and hematocrit levels in experimental rats. *A*: representative images of HIF-1α staining in kidneys (*top*) and hearts (*bottom*) of rats. HIF-1α was observed in the nuclei of tubular cells and cardiomyocytes in enarodustat-treated rats. An image of high magnification is shown in the *inset*. Original magnification: ×200 (*top*) and ×400 (*bottom*). Bar = 50 μm. *B*: hematocrit levels at −2, 2, 4, and 6 wk ($n = 5$ for sham, $n = 13$ for remnant kidney (RK) + vehicle, and $n = 7$ for RK + enarodustat). Data are expressed as means ± SE. $^*P < 0.05$, $^{**}P < 0.01$, and $^{***}P < 0.001$. ns, Not significant.

mitochondria were measured by tracing at least 3 randomly selected electron micrographs of longitudinally arranged cardiomyocytes using National Institutes of Health ImageJ software.

TUNEL assay. Apoptotic cells in the heart and kidney were detected using a TACS 2 TdT-Blue Label In Situ Apoptosis Detection Kit (Trevigen, Gaithersburg, MD).

Real-time PCR analysis. RNA was isolated by RNA iso (Takara, Shiga, Japan) and reverse transcribed with RT Master Mix (Takara). cDNA was subjected to real-time PCR using THUNDERBIRD qPCR Mix (Toyobo, Osaka, Japan) and a CFX96 Real Time System (Bio-Rad, Hercules, CA). Data were analyzed using the $\Delta\Delta C_t$ method and normalized by β-actin. Primer sequences are shown in Supplemental Table S1 (available online at https://doi.org/10.6084/m9.figshare.11312171.v1).

Measurement of plasma IL-6 and TNF-α levels. Plasma concentrations of IL-6 and TNF-α were measured using the T helper (Th)1 and Th2 Bioplex cytokine kit (Bio-Rad).

Cell culture. P19CL6 cells (RIKEN BRC) were cultured in α-MEM (GIBCO, Carlsbad, CA) supplemented with 10% FBS (13). To induce differentiation into cardiomyocytes, P19CL6 cells were plated at a density of 1.6×10^5 cells/well in a six-well format and cultured with growth medium containing 1% DMSO for 16 days. After differentiation, medium was changed to serum-free medium for 24 h, and cells were treated with ANG II (1 μM, 24 h, Calbiochem, San Diego, CA), and with enarodustat (10 μM, 24 h) or vehicle (0.1% DMSO; see Fig. 9A).

Statistical analysis. Results are expressed as means ± SE. Data were assessed with one-way ANOVA with Dunnett's post hoc test. Changes in SBP, BUN, serum creatinine levels, and urinary protein excretion over time were analyzed with one-way ANOVA for repeated measures with a Tukey's post hoc test (see Supplemental Fig. S1 available online at https://doi.org/10.6084/m9.figshare.11312189.v1). *P* values of <0.05 were considered statistically significant. Analyses were conducted using GraphPad Prism software (version 7.0, GraphPad Software, La Jolla, CA).

RESULTS

HIF stabilization by PHD inhibition. HIF activation was confirmed by HIF-1α immunohistochemistry. HIF-1α was observed in the nuclei of tubular cells and cardiomyocytes in the RK + enarodustat group (Fig. 2*A*). Hematocrit levels were significantly lower in the RK + vehicle group compared with the sham group after 4 wk. Hematocrit levels in the RK + enarodustat group were significantly higher than those in the RK + vehicle group at 6 wk (Fig. 2*B*), which suggested enarodustat-induced EPO production.

Results of physiological parameters. There was no significant difference in body weight and SBP between the RK + vehicle and RK + enarodustat groups (Table 1). Urinary Na^+

Table 1. *Physiological parameters of experimental animals*

	Sham ($n = 9$)	RK + Vehicle ($n = 18$)	RK + Enarodustat ($n = 14$)
Body weight, g			
Week 6	547 ± 11	510 ± 10[a]	506 ± 10
Heart weight/body weight, mg/g			
Week 6	2.84 ± 0.12	3.31 ± 0.1[a]	3.45 ± 0.19
Systolic blood pressure, mmHg			
Week 2	129 ± 6	185 ± 11[c]	179 ± 4
Week 4	132 ± 6	189 ± 11[c]	177 ± 5
Week 6	138 ± 5	177 ± 10[b]	169 ± 4
Blood urea nitrogen, mg/dL			
Week 2	17.3 ± 0.7	61.0 ± 5.1[d]	50.1 ± 4.8
Week 4	20.0 ± 0.7	61.3 ± 4.2[d]	47.9 ± 4.1[e]
Week 6	18.7 ± 0.8	55.6 ± 5.4[d]	46.8 ± 4.6
Creatinine, mg/dL			
Week 2	0.34 ± 0.03	1.11 ± 0.09[c]	0.88 ± 0.08
Week 4	0.34 ± 0.04	1.11 ± 0.09[c]	0.86 ± 0.10
Week 6	0.38 ± 0.03	1.04 ± 0.13[c]	0.83 ± 0.07
Urinary protein excretion, mg/day			
Week 2	9.3 ± 1.5	29.2 ± 8.4	39.1 ± 12.7
Week 4	9.8 ± 2.2	38.1 ± 7.2	32.6 ± 10.3
Week 6	8.9 ± 1.1	48.8 ± 9.2[a]	40.8 ± 13.0

Data are expressed as means ± SE. For heart weight/body weight, $n = 5$ for sham, $n = 10$ for remnant kidney (RK) + vehicle, and $n = 5$ for RK + enarodustat; for systolic blood pressure, $n = 5$ for sham, $n = 8$ for RK + vehicle, and $n = 9$ for RK + enarodustat. [a]$P < 0.05$ vs. sham; [b]$P < 0.01$ vs. sham; [c]$P < 0.001$ vs. sham; [d]$P < 0.0001$ vs. sham; [e]$P < 0.05$ vs. RK + vehicle.

and K^+ excretion was not significantly different between RK groups (see Supplemental Table S2, available online at https://doi.org/10.6084/m9.figshare.11312183.v1).

Enarodustat ameliorated cardiac hypertrophy and fibrosis. The ratio of heart weight to body weight was higher in the RK + vehicle group compared with the sham group, whereas the ratio was unchanged by enarodustat treatment (Table 1). In an echocardiographic analysis, IVSTd and LVPWTd increased significantly in the RK + vehicle group, and they were significantly suppressed by enarodustat (Fig. 3, *A*–*C*). In contrast, LVIDd, LVIDs, FS, and heart rate were not different among groups (Fig. 3, *D*–*G*). These data suggest that systolic and diastolic dysfunction was not evident in the present study.

Renal fibrosis was exacerbated in the RK groups, and it was less severe in the enarodustat-treated group than in the vehicle-treated group (Fig. 4, *A*, *B*, *D*, and *E*). Cross-sectional areas of cardiomyocytes were enlarged in the RK groups and attenuated in the enarodustat-treated group (Fig. 4, *C* and *F*). The ratio of β-myosin heavy chain (MHC) to α-MHC mRNA expression, as a surrogate measure for cardiac hypertrophy (23), was higher in the RK group compared with the sham group, which was suppressed by enarodustat treatment (Fig. 4*G*).

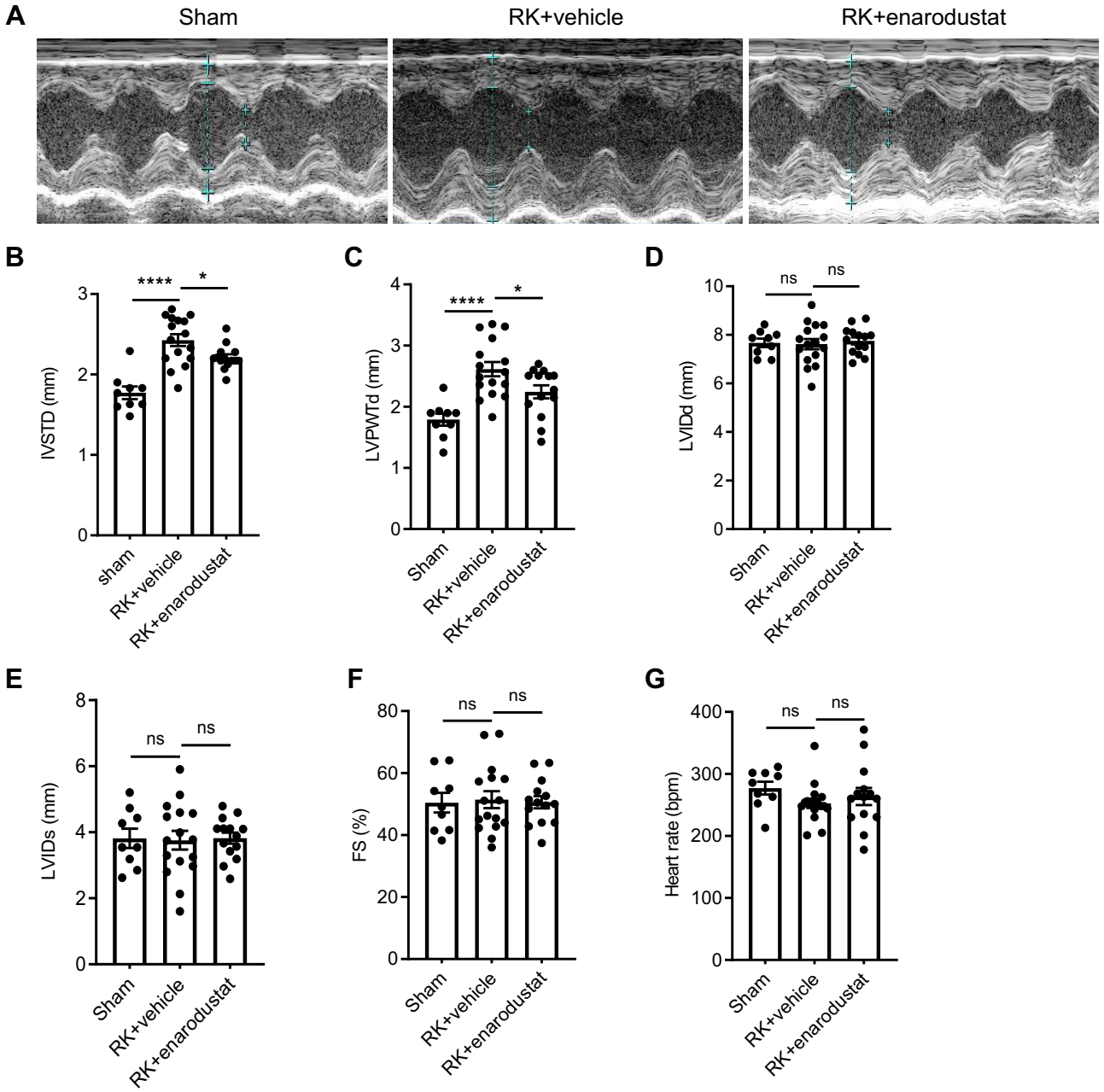

Fig. 3. Echocardiographic analyses and the ratio of heart weight to body weight. *A*: representative images of M-mode transthoracic echocardiographic analyses. *B* and *C*: measurement of interventricular septum thickness (IVSTd; *B*) and left ventricular posterior wall thickness (LVPWTd; *C*). *D*–*G*: measurement of left ventricular internal diameter at diastole (LVIDd; *D*), left ventricular internal diameter at systole (LVIDs; *E*), fractional shortening (FS; *F*), and heart rate (*G*) [$n = 9$ for sham, $n = 16$ for remnant kidney (RK) + vehicle, and $n = 14$ for RK + enarodustat]. Data are expressed as means ± SE. $^*P < 0.05$ and $^{****}P < 0.0001$. ns, Not significant.

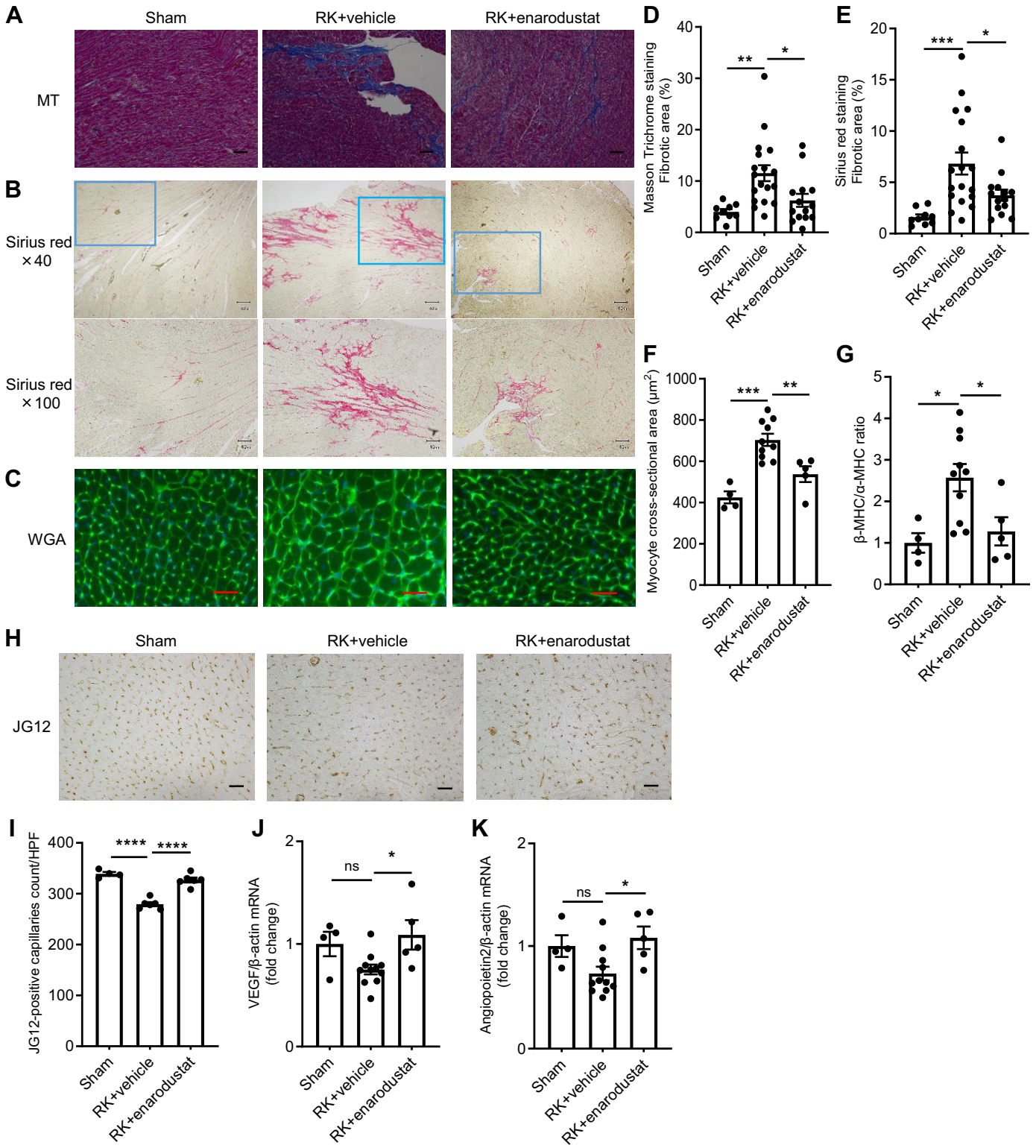

Fig. 4. Effects of enarodustat on cardiac hypertrophy, fibrosis, and angiogenesis. *A* and *B*: representative images of Masson trichrome (MT) staining (*A*) and Sirius red staining (*B*) of the heart. Original magnification: ×200 (*A*), ×40 (*B*, *top*), and ×100 (*B*, *bottom*). *C*: representative images of wheat germ agglutinin (WGA) staining. *D* and *E*: percentage of blue area in Masson trichrome staining (*D*) and picrosirius red-positive area (*E*, ×100) [$n = 9$ for sham, $n = 18$ for remnant kidney (RK) + vehicle, and $n = 14$ for RK + enarodustat]. *F*: quantification of myocyte cross-sectional area ($n = 4$ for sham, $n = 10$ for RK + vehicle, and $n = 5$ for RK + enarodustat). *G*: relative mRNA expression of β-myosin heavy chain (MHC) and α-MHC. The ratio of β-MHC to α-MHC expression levels was calculated as a surrogate for cardiac hypertrophy (real-time PCR: $n = 4$ for sham, $n = 10$ for RK + vehicle, and $n = 5$ for RK + enarodustat). *H*: representative images of JG12 staining of the heart. Original magnification: ×400. *I*: the number of JG12-positive microvascular capillaries was expressed as count/field ($n = 4$ for sham, $n = 6$ for RK + vehicle, and $n = 6$ for RK + enarodustat). *J* and *K*: relative mRNA expression of proangiogenic genes in the heart was quantified by real-time PCR ($n = 4$ for sham, $n = 10$ for RK + vehicle, and $n = 5$ for RK + enarodustat). Data are expressed as means ± SE. $^*P < 0.05$, $^{**}P < 0.01$, $^{***}P < 0.001$, and $^{****}P < 0.0001$. Bar = 50 μm. ns, Not significant.

Enarodustat preserved capillary density in the heart and activated proangiogenic factors. The number of JG12-positive endothelial capillaries was significantly less in the RK + vehicle group than in the sham group, and this reduction was reversed with enarodustat treatment (Fig. 4, *H* and *I*). Enarodustat treatment restored VEGF and angiopoietin-2 mRNA levels in the heart (Fig. 4, *J* and *K*).

Enarodustat suppressed cardiac apoptosis and macrophage infiltration. The percentage of TUNEL-positive nuclei was significantly higher in the RK + vehicle group than in the sham group, which was reduced by enarodustat (Fig. 5, *A* and *B*). The expression level of Bcl-2 was significantly upregulated by enarodustat treatment, whereas there was no significant difference in Bax expression (Fig. 5, *C* and *D*). Furthermore, macrophage infiltration was remarkably ameliorated by enarodustat treatment (Fig. 5, *E* and *F*). mRNA expression of M1 macrophage markers [TNF-α, IL-6, and chemokine (C-C motif) ligand 2 (CCL2)] and M2 macrophage markers [arginase-1 and mannose receptor, C type 1 (Mrc-1)] did not change significantly by enarodustat (Fig. 5*G*).

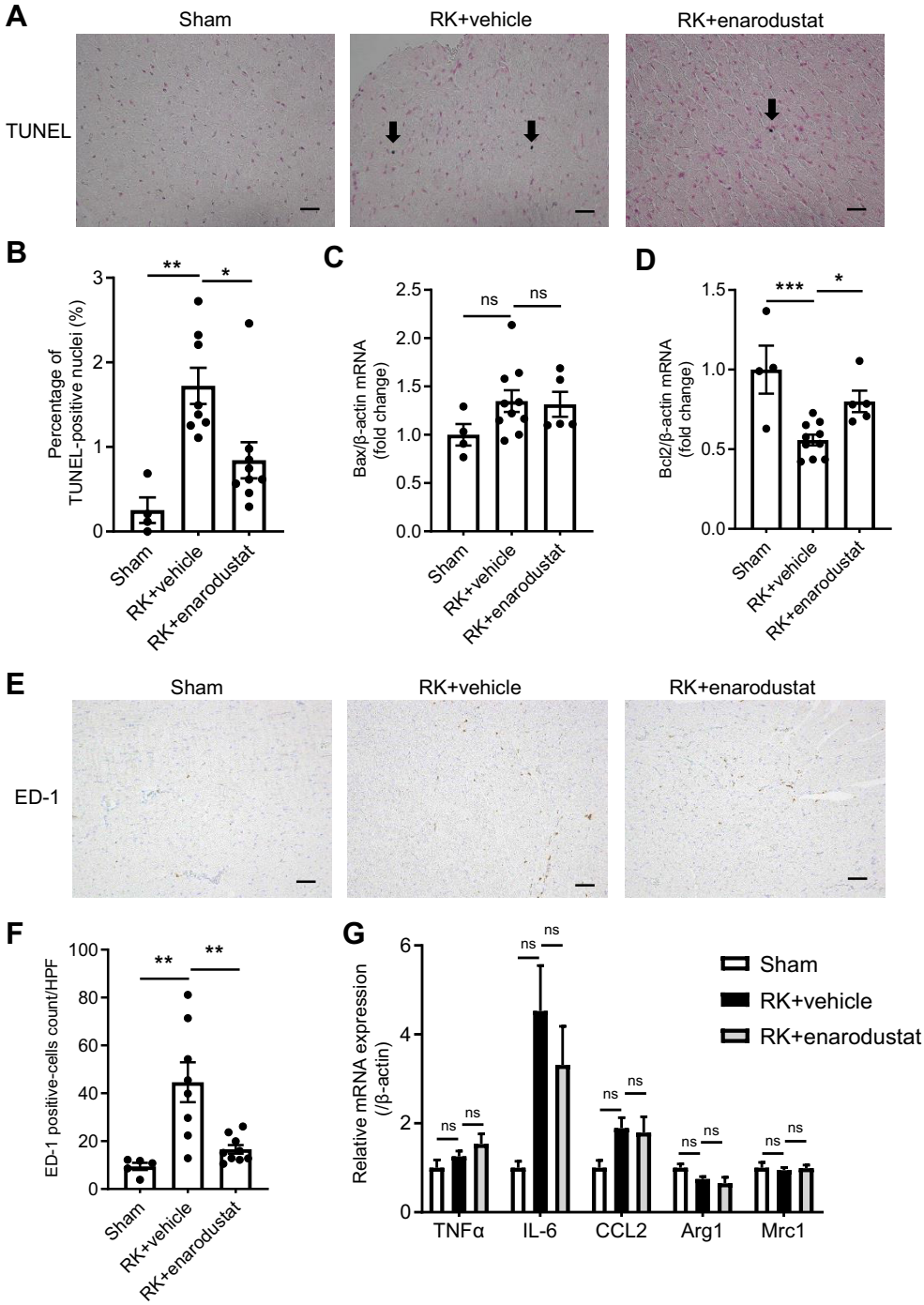

Fig. 5. Effects of enarodustat on cardiac apoptosis and macrophage infiltration. *A*: representative images of TUNEL staining of the heart. Apoptotic cardiomyocytes (arrows) were detected. Original magnification: ×200. *B*: percentage of TUNEL-positive nuclei [$n = 4$ for sham, $n = 8$ for remnant kidney (RK) + vehicle, and $n = 9$ for RK + enarodustat]. *C* and *D*: relative mRNA expression of apoptosis-related genes in the heart was quantified by real-time PCR ($n = 4$ for sham, $n = 10$ for RK + vehicle, and $n = 5$ for RK + enarodustat). *E*: representative images of ED-1 staining of the heart. Original magnification: ×200. *F*: number of infiltrating macrophages expressed as count/field ($n = 5$ for sham, $n = 8$ for RK + vehicle, and $n = 9$ for RK + enarodustat). *G*: relative mRNA expression of inflammation-related genes was quantified by real-time PCR ($n = 4$ for sham, $n = 10$ for RK + vehicle, and $n = 5$ for RK + enarodustat). CCL2, chemokine (C-C motif) ligand 2; Arg1, arginase 1; Mrc1, mannose receptor, C type 1. Data are expressed as means ± SE. $^{*}P < 0.05$, $^{**}P < 0.01$, and $^{***}P < 0.001$. Bar = 50 μm. ns, Not significant.

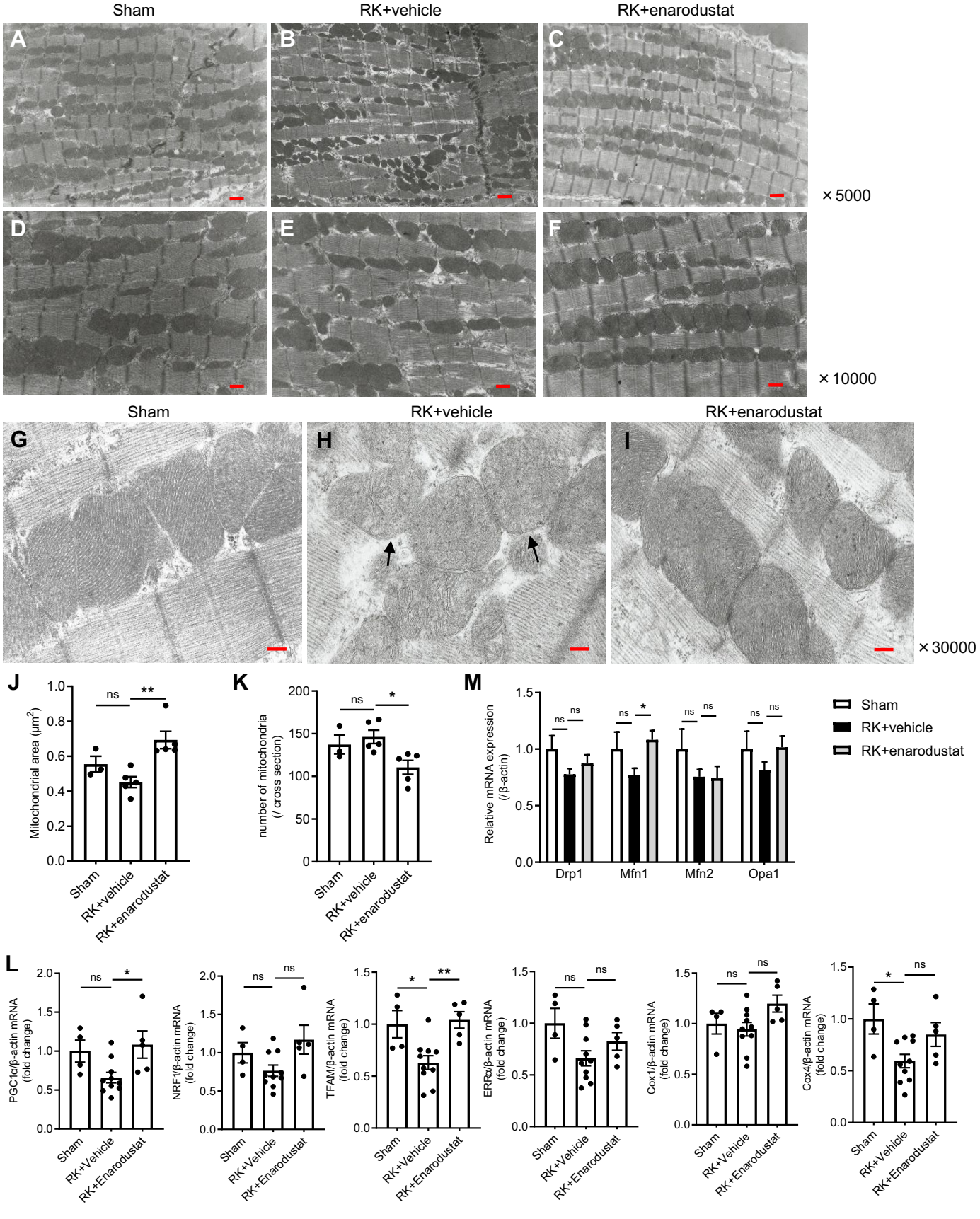

Enarodustat modulated mitochondria biogenesis, dynamics, and mitochondrial volume in the heart. We then evaluated the expression levels of genes involved in mitochondrial biogenesis (Fig. 6*L*). mRNA levels of peroxisome proliferator-activated receptor-γ coactivator (PGC)-1α were significantly upregulated by enarodustat and similar to those in the sham group. PGC-1α modulates mitochondrial biogenesis by directly coactivating transcriptional factors such as nuclear respiratory factor (NRF) and estrogen-related receptor α (ERRα; see Ref. 33). However, mRNA levels of NRF1 and ERRα were unchanged by enarodustat (Fig. 6*L*). In contrast, mRNA expression of mitochondrial transcription factor A (TFAM), the key regulator of mitochondrial DNA replication and transcription, was less in the RK + vehicle group than the sham group and was reversed with enarodustat treatment. Cytochrome *c* oxidase (COX) is a key enzyme in the mitochondrial respiratory chain, and the expression level of COX4, but not COX1, was less in the RK + vehicle group than the sham group but was similar in the RK + vehicle and RK + enarodustat group (Fig. 6*L*). Fusion is regulated by mitofusin (Mfn)1, Mfn2, and optic atrophy 1 (Opa1), whereas fission is regulated by dynamin-related protein 1 (Drp1; see Ref. 28). Mfn1 mRNA was induced by enarodustat, whereas Drp1, Mfn2, and Opa1 levels were unchanged (Fig. 6*M*). Morphological analyses by transmission electron microscopy indicated comparable mitochondrial masses in the RK + vehicle and sham groups and a significant increase in response to enarodustat (Fig. 6*J*). In addition, the number of mitochondria was less in the enarodustat-treated group than in the vehicle-treated group (Fig. 6*K*). At high magnification (×30,000), mitochondria cristae disruption appeared less by enarodustat treatment (Fig. 6, *G–I*).

Enarodustat had beneficial effects on renal pathology. Glomerular sclerosis and tubulointerstitial injury were evident in RK groups. Tubulointerstitial injury was significantly improved by enarodustat, whereas glomerular sclerosis was unchanged (Fig. 7, *A*, *D*, and *E*). Enarodustat attenuated renal tubulointerstitial fibrosis (Fig. 7, *B*, *C*, and *F*). Furthermore, enarodustat markedly suppressed the expression of profibrotic genes, including collagen type III-α_1 and transforming growth factor-β (Fig. 7, *G* and *H*). Loss of glomerular capillaries was observed in the RK + vehicle group, which was reversed with enarodustat treatment (Fig. 7, *I* and *J*).

The number of ED1-positive cells in the tubulointerstitium increased in the RK + vehicle group, which was remarkably less in the enarodustat-treated group (Fig. 8, *A* and *B*). Expression levels of TNF-α, IL-6, and CCL2 in the kidney were significantly reduced by enarodustat treatment, whereas the expression of arginase-1 and Mrc1 was unchanged (Fig. 8*C*). Plasma TNF-α concentration was 2,634 ± 384 pg/mL in the RK + vehicle group ($n = 15$) and 1,772 ± 481 pg/mL in the RK + enarodustat group ($n = 11$, $P = 0.32$). Plasma IL-6 concentration was 2,425 ± 378 pg/mL in the RK + vehicle group ($n = 14$) and 2,168 ± 553 pg/mL in the RK + enarodustat group ($n = 8$, $P = 0.92$). The number of TUNEL-positive cells was also significantly less in the RK + enarodustat group compared with that in the RK + vehicle group, suggesting an antiapoptotic role of enarodustat (Fig. 8, *D* and *E*). Expression of Bax was repressed by enarodustat (Fig. 8*F*).

In contrast to the histological improvements, there was no significant difference in BUN, serum creatinine levels, and urinary protein excretion between the vehicle-treated and enarodustat-treated groups throughout the experimental course except for BUN at 4 wk (Table 1). Individual data of SBP, BUN, serum creatinine levels, and urinary protein excretion at −2, 2, 4, and 6 wk are shown in Supplemental Fig. S1.

Enarodustat suppressed mRNA expression of hypertrophic markers in P19CL6 cells. We next analyzed the effect of enarodustat on ANG II-induced cardiac hypertrophy using differentiated P19CL6 cells. Differentiation into cardiac myocytes was confirmed by GATA4 mRNA expression. The expression level of GATA4 was markedly upregulated at *day 18* (Fig. 9*B*), and there was no significant difference among the three groups (Fig. 9*C*). HIF activation was confirmed by VEGF upregulation (Fig. 9*D*). mRNA expression levels of the hypertrophy markers, such as atrial natriuretic peptide gene and the β-MHC/α-MHC ratio, were higher in the ANG II + vehicle group compared with the control group, which were markedly attenuated by enarodustat (Fig. 9, *E* and *F*).

DISCUSSION

To our knowledge, this is the first report showing that activation of HIF ameliorates cardiac hypertrophy and fibrosis in association with restored capillary density and improved mitochondrial morphology in the 5/6 nephrectomy model. Because patients with CKD often reveal a progressive decrease in NO availability that is associated with reduced cardiac output and dose-dependent hypertension, we used the RK model with a NO synthase inhibitor (L-NNA) as previously described by Bongartz et al. (7). However, it is important to note that our study design was different from that of Bongartz et al. The left renal artery branch ligation preceded the right-sided uninephrectomy in our study, whereas right-sided uninephrectomy preceded the left-sided polectomy using surgical resection in their study. The ligation model usually causes overt hypertension and glomerular injury. In addition, Bongartz et al. used Lewis rats, which were considered to be resistant to subtotal nephrectomy and NO depletion (44), and gave the rats a high-salt diet for a longer experimental period, whereas we used Sprague-Dawley rats for the shorter period. Among the differences mentioned above, there is a possibility

Fig. 6. Mitochondrial morphology and results of mitochondrial biogenesis and dynamics in the heart. *A–I*: representative electron microscopy from sham, remnant kidney (RK) + vehicle, and RK + enarodustat rats hearts. Original magnification: ×5,000, bar = 1 μm (*A–C*); ×10,000, 500 nm (*D–F*); and ×30,000; and 200 nm (*G–I*). Note that mitochondria cristae disruption (arrows) appeared less in the enarodustat-treated group than in the vehicle-treated group at high magnification (×30,000). *J* and *K*: quantification of the area of mitochondria (*J*) and number of mitochondria (*K*) obtained by transmission electron microscopy images at ×5,000 magnification ($n = 5$ in the RK group and $n = 3$ in the sham group). *L*: relative mRNA expression of mitochondrial biogenesis-related genes [peroxisome proliferator-activated receptor-γ coactivator (PGC)-1α, nuclear respiratory factor (NRF)1, transcription factor A (TFAM), estrogen-related receptor α (ERRα), cytochrome *c* oxidase (COX)-1, and COX4] was quantified by real-time PCR. *M*: relative mRNA expression of mitochondrial dynamics-related genes [dynamin-related protein 1 (Drp1), mitofusin (Mfn)1, Mfn2, and optic atrophy 1 (Opa1)] was quantified by real-time PCR ($n = 4$ for sham, $n = 10$ for RK + vehicle, and $n = 5$ for RK + enarodustat). Data are expressed as means ± SE. *$P < 0.05$ and **$P < 0.01$. ns, Not significant.

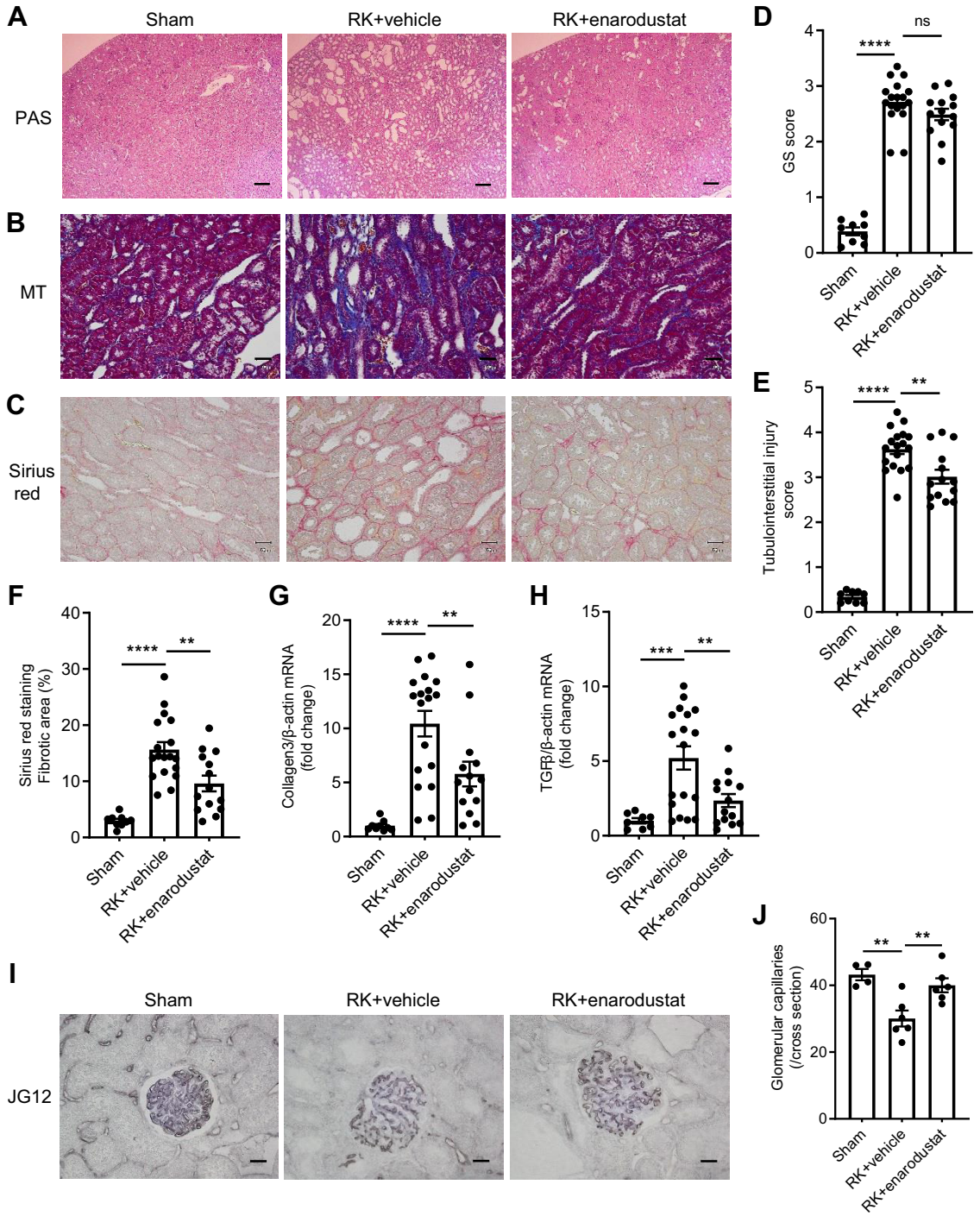

Fig. 7. Effects of enarodustat on glomerular and tubulointerstitial injury, and renal capillary density. *A–C*: representative images of periodic acid-Schiff (PAS) staining (*A*), Masson trichrome (MT) staining (*B*), and Sirius red staining (*C*) of the kidney. Original magnification: ×40, bar = 250 μm (*A*), ×200, bar = 50 μm (*B* and *C*). *D* and *E*: semiquantitative scoring of glomerular sclerosis (GS; *D*) and tubulointerstitial injury (*E*). *F*: percentage of picrosirius red-positive area in the cortical area [$n = 9$ for sham, $n = 18$ for remnant kidney (RK) + vehicle, and $n = 14$ for RK + enarodustat]. *G* and *H*: relative mRNA expression of profibrotic genes in the kidney was quantified by real-time PCR ($n = 9$ for sham, $n = 18$ for RK + vehicle, and $n = 14$ for RK + enarodustat). *I*: representative images of JG12 staining of the kidney. Original magnification: ×400, bar = 50 μm. *J*: number of JG12-positive microvascular capillaries as count/field ($n = 4$ for sham, $n = 6$ for RK + vehicle, and $n = 6$ for RK + enarodustat). Data are expressed as means ± SE. $^{**}P < 0.01$, $^{***}P < 0.001$, and $^{****}P < 0.0001$. ns, Not significant.

that the shorter experimental period in our study is the most attributable to the absence of cardiac dysfunction.

Cardiac hypertrophy was evidenced by an increased heart weight-to-body weight ratio, cardiomyocyte size by WGA staining, and expression of cardiac hypertrophy-related marker as well as echocardiographic analyses. All of these parameters, except for the heart weight-to-body weight ratio, were significantly less by enarodustat treatment. Although the heart

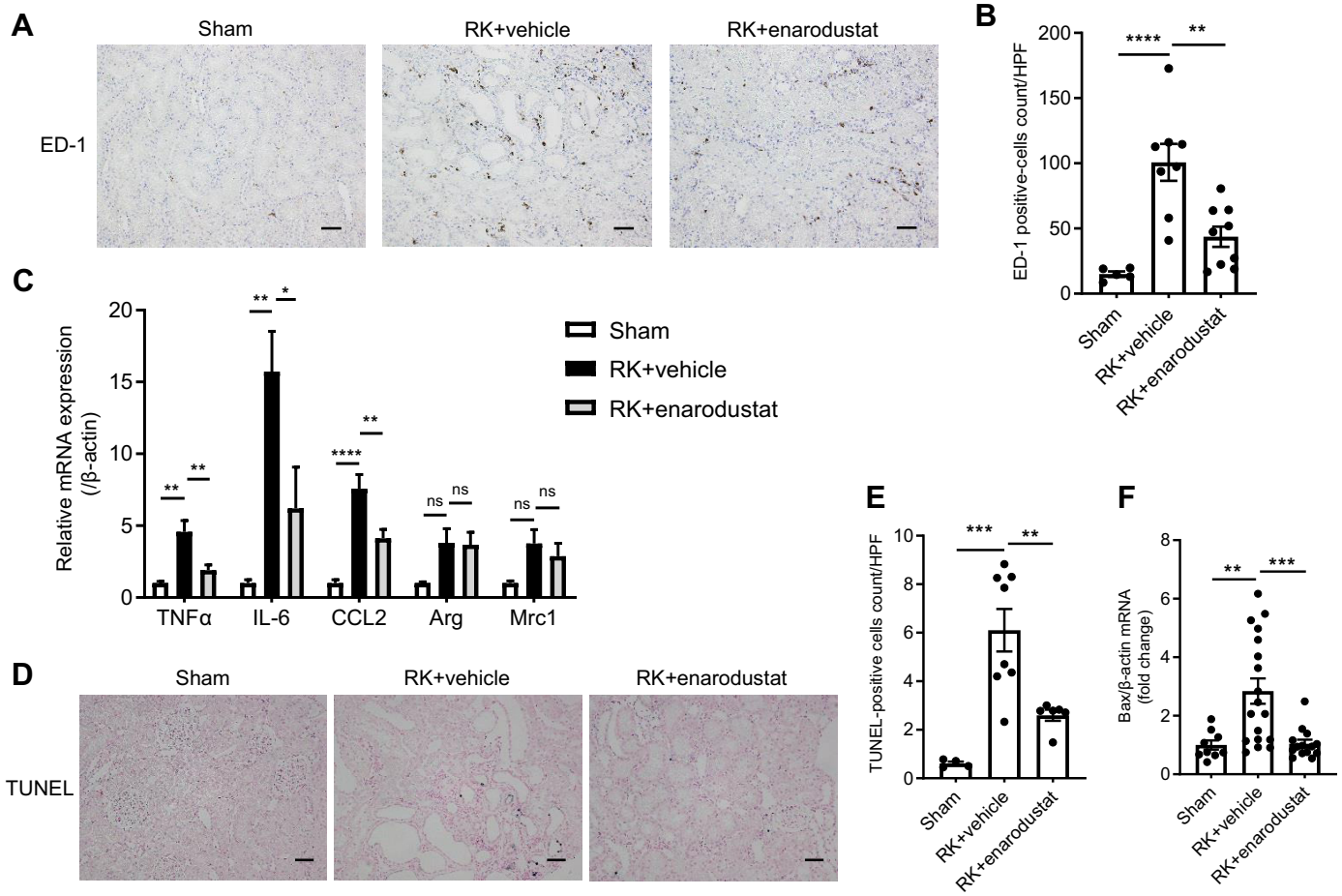

Fig. 8. Effects of enarodustat on renal macrophage infiltration and apoptosis. *A*: representative images of ED-1 staining of the kidney. Original magnification: ×200. *B*: number of infiltrating macrophages as count/field [$n = 5$ for sham, $n = 8$ for remnant kidney (RK) + vehicle, and $n = 9$ for RK + enarodustat]. *C*: relative mRNA expression of inflammation-related genes [TNF-α, IL-6, chemokine (C-C motif) ligand 2 (CCL2), arginase (Arg)1, and mannose receptor, C type 1 (Mrc1)] in the kidney was quantified by real-time PCR ($n = 9$ for sham, $n = 18$ for RK + vehicle, and $n = 14$ for RK + enarodustat). *D*: representative images of TUNEL staining of the kidney. Original magnification: ×200. *E*: number of TUNEL-positive cells expressed as count/field ($n = 4$ for sham, $n = 8$ for RK + vehicle, and $n = 6$ for RK + enarodustat). *F*: Bax mRNA expression in the kidney was quantified by real-time PCR ($n = 9$ for sham, $n = 18$ for RK + vehicle, and $n = 14$ for RK + enarodustat). Data are expressed as means ± SE. $^*P < 0.05$, $^{**}P < 0.01$, $^{***}P < 0.001$, and $^{****}P < 0.0001$. Bar = 50 μm. ns, Not significant.

weight-to-body weight ratio is often used to assess the extent of cardiac hypertrophy, it may also disproportionately reflect body weight loss that occurs when establishing this model. Alternative measures such as the heart weight-to-tibia length ratio may have provided a more accurate marker of cardiac hypertrophy.

LVH is accompanied by myocardial fibrosis (22, 32). Although hypertension is a risk factor for CKD and CVD, attenuation of LVH and myocardial fibrosis in CKD is partly independent of blood pressure (39, 45). In line with these studies, our data showed that enarodustat attenuated cardiac remodeling without altering blood pressure. Correction of hemoglobin concentrations by treatment with recombinant human EPO (rHuEPO) results in partial regression of LVH in patients with CKD (30). Because PHD inhibitors increase hemoglobin levels (43), these inhibitors might also be beneficial in treating anemia in patients with CKD and end-stage renal disease with cardiac hypertrophy. This hypothesis should be tested in future clinical studies.

In vitro, mRNA expression of cardiac hypertrophy markers, namely atrial natriuretic peptide and the β-MHC/α-MHC ratio, was suppressed significantly by enarodustat, which also provides mechanistic insight into a previously unrecognized relationship between hypertrophic responses and HIF activation.

The mechanism of cardioprotection by HIF activation involves restored capillary density, altered Ca^{2+} handling, and a metabolic switch toward glucose consumption (51). In a model of transverse aortic constriction, sustained pressure overload caused the accumulation of p53, which inhibited HIF-1 activity and impaired cardiac angiogenesis (34). In this respect, preserved cardiac vascularization in the present study could also contribute to cardioprotection. Furthermore, restoration, rather than uncontrolled growth, of capillaries and vascular factors by enarodustat might provide reassuring view on the safety of PHD inhibitors for angiogenesis-related diseases such as diabetic retinopathy and cancer (12).

An imbalance in mitochondrial fusion and fission leads to apoptosis (42). Morphological analyses by transmission electron microscopy indicated a significant increase in mitochondrial mass by enarodustat, to be consistent with a previous report (17). Mitochondria in the failing rat hearts are generally small and fragmented, albeit dynamic to some extent (8, 48).

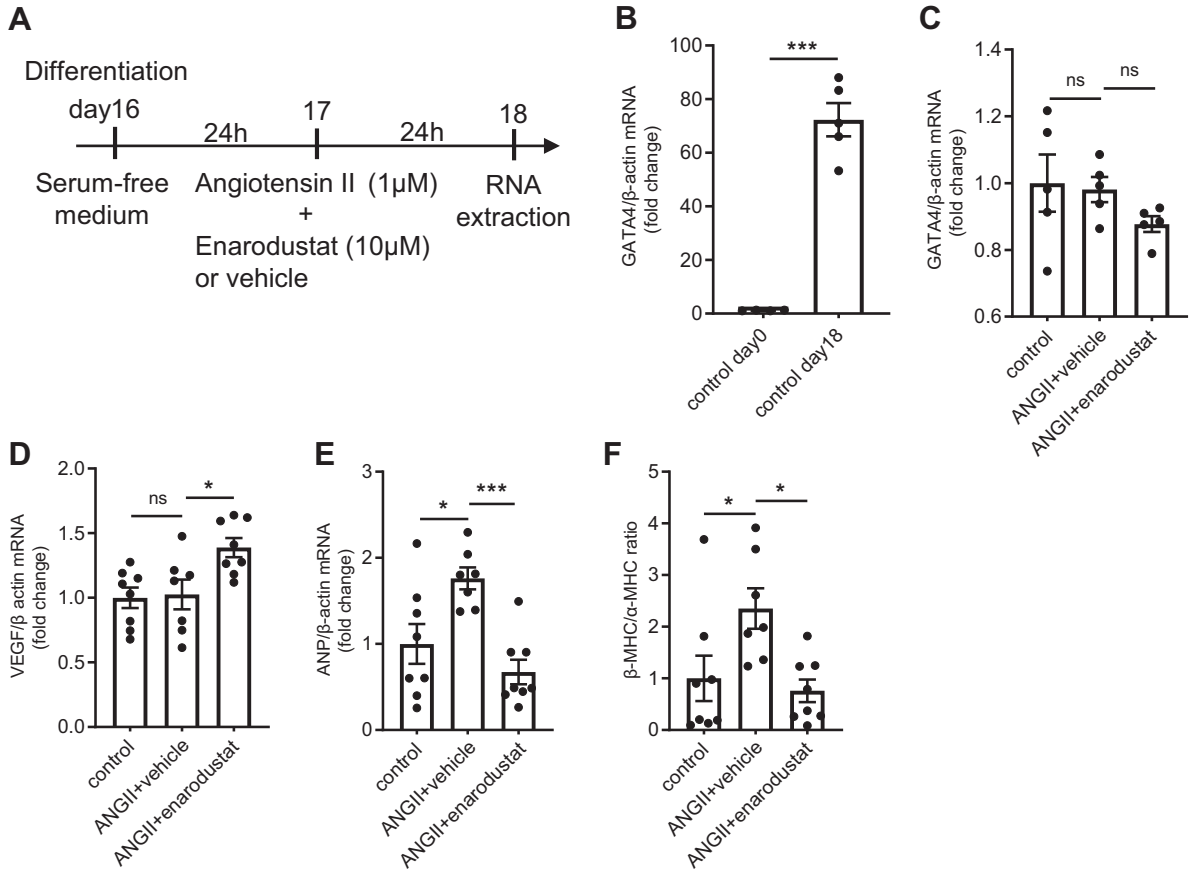

Fig. 9. Effect of enarodustat on mRNA expression of hypertrophic markers in P19CL6 cells. *A*: experimental design for *B–F*. P19CL6 cells were treated with ANG II (1 μM, 24 h) and with enarodustat (10 μM, 24 h) or vehicle (0.1% DMSO). RNA was then extracted. *B* and *C*: relative mRNA expression of GATA4 quantified by real-time PCR. Note that the upregulation of GATA4 at *day 18* suggests cardiac differentiation by 1% DMSO. Data in *B* were analyzed with a Student's *t* test (2-tailed). *D*: relative mRNA expression of VEGF quantified by real-time PCR. *E* and *F*: relative mRNA expression of hypertrophy marker genes atrial natriuretic peptide (ANP; *E*) and β-myosin heavy chain (β-MHC) by real-time PCR. The β-MHC/α-MHC ratio (*F*) was calculated accordingly ($n = 5–8$ in each group). Data are expressed as means ± SE. $^*P < 0.05$ and $^{***}P < 0.001$. ns, Not significant.

Mitochondria in compensated myocardial hypertrophy and heart failure in humans were increased in number and appeared smaller than those in the controls (29). In addition to structural changes, we observed gene expression changes associated with mitochondrial biogenesis. PGC-1α acts upstream of Nrf1/Nrf2 and TFAM and has the capacity to increase mitochondrial DNA levels and mitochondrial mass (52). It is not clear whether upregulation of PGC-1α is a direct effect of HIF activation or reflects the net cardioprotective effects secondary to HIF activation because HIF typically inhibits mitochondrial biogenesis by reducing PGC-1 (36). However, FG4592, a PHD inhibitor, improved mitochondrial function by inducing HIF-1α-AMP-activated protein kinase-PGC-1α signaling after neuronal injury (21), and our observation is in keeping with these preceding studies.

Inflammation is also an important consideration in cardiac hypertrophy. The number of cardiac ED1-positive cells was significantly less in the RK + enarodustat group than in the RK + vehicle group, whereas mRNA expression of proinflammatory cytokines such as TNFα, IL-6, and CCL2 was not reduced by enarodustat. As gene expression of inflammatory cytokines peaked at *day 4–7* in an ANG II-mediated cardiac fibrosis model (49), possible explanation of the discrepancy in these results is that mRNA expression of proinflammatory cytokines had already peaked and declined at the time of measurement.

In kidneys, attenuation of fibrosis by a PHD inhibitor was accompanied by decreased macrophage infiltration and proinflammatory cytokine release, which is consistent with the results of a previous study (46). However, in contrast to previous reports that showed kidney protection by HIF activation in the remnant kidney, we did not observe improvement of proteinuria and creatinine levels during the observation period in our study. These differences may arise from distinct protocols such as the use of NO synthase inhibitors and evaluation time points. Plasma creatinine levels and urinary protein excretion were significantly reduced by cobalt chloride treatment at 9 wk after 5/6 nephrectomy, whereas there was no significant difference in these parameters at 5 wk (46). Therefore, we speculate that measurement in later phases may have revealed an improvement of proteinuria and renal dysfunction by enarodustat. In contrast, another study of 5/6 nephrectomy using L-mimosine as a PHD inhibitor demonstrated that activation of HIF at *weeks 2–12* aggravated renal function and histology, whereas treatment at *weeks 4–12* ameliorated injury (53). Therefore, it is alternatively possible that initiation of en-

arodustat treatment at a later time point might have reduced proteinuria and injury.

In the pathogenesis of 5/6 nephrectomy, previous reports have emphasized blood pressure-dependent injury, such as impaired autoregulation and glomerular blood pressure transmission, and blood pressure-independent injury, including nonhemodynamic profibrotic signaling and efferent constriction (6). Although the effects of PHD inhibitors on blood pressure have not been fully elucidated, it has been demonstrated that silencing of PHD2 gene expression in the renal medulla induced HIF-1α target genes, such as heme oxygenase-1 and COX-2, enhanced natriuresis, and, consequently, attenuated salt-sensitive hypertension in Dahl S rats (54). Besides, previous studies have suggested that the induction of HIF-1α may provide blood pressure-independent renoprotection in the 5/6 ablation model (41, 46). Our data did not show a difference in natriuresis by enarodustat, and the neutral effect of a PHD inhibitor on blood pressure might account for the lack of amelioration in proteinuria by enarodustat. Alternatively, the present findings suggest that the cardioprotective effects of enarodustat are independent of kidney function. Because the development of pathological cardiac hypertrophy occurs even in early stage nonuremic CKD (14), starting PHD inhibitor treatment during early CKD might be a potential therapeutic strategy for protecting cardiac hypertrophy.

There are several limitations of our study. First, we did not observe changes in hearts and kidneys except at 6 wk after 5/6 nephrectomy. Because cardiac hypertrophy initially occurs as an adaptive response and then develops into pathological cardiac hypertrophy, results of our analyses might change by evaluation of a different phase of cardiac hypertrophy. Furthermore, rats received the enarodustat treatment at −2 to 6 wk, and another timing of PHD inhibitor administration was not performed in the present study. Second, our study design missed a sham-operated group treated with enarodustat, which could reveal potential interaction between treatment and disease. Third, we did not check the *E*/*e′* ratio, which is the parameter to assess diastolic function of heart failure with preserved ejection fraction (10).

In conclusion, the present study showed that activation of HIF by a PHD inhibitor reduced cardiac hypertrophy, ameliorated myocardial fibrosis in association with restored capillary density, and improved mitochondrial morphology in a RK model. In kidneys, amelioration of renal fibrosis by PHD inhibitors was associated with decreased proinflammatory cytokine expression, apoptosis, and restored capillary density. The PHD inhibitor appeared to show beneficial effects on cardiovascular complications caused by CKD. Future clinical trials for a longer observation period will be required to evaluate the potential for cardiovascular complications in CKD patients receiving PHD inhibitors.

ACKNOWLEDGMENTS

We thank Dr. Yu Shimizu (The University of Tokyo) for technical advice and Kahoru Amitani and Satoru Fukuda (The University of Tokyo) for technical support.

GRANTS

The work was supported by Japan Society for the Promotion of Science Grants-in-Aid for Scientific Research 18H02824 (to M. Nangaku) and 17K09688 (to T. Tanaka) and Biological and Pharmacological Research Laboratories, Central Pharmaceutical Research Institute, Japan Tobacco Incorporated.

DISCLOSURES

M. Nangaku has received honoraria, advisory fees, or research funding from Kyowa-Kirin, Akebia, Astellas, Chugai, GSK, JT, Taisho-Toyama, Torii, Mitsubishi-Tanabe, Daiichi-Sankyo, Bayer, and Boehringer Ingelheim. T. Tanaka has received research grant from JT. L. Uchida, H. Saito, M. Sugahara, K. Fukui, and T. Wakashima declared no competing interests. Enarodustat was provided by Japan Tobacco Incorporated.

AUTHOR CONTRIBUTIONS

L.U., T.T., and M.N. conceived and design the research; L.U., H.S, M.S., K.F, and T.W. performed experiments; L.U. and T.T. analyzed data; L.U, T.T, and M.N. interpreted the results of experiments; L.U. and T.T. prepared the figures and drafted the manuscript; L.U., T.T., and M.N. edited and revised the manuscript; L.U., T.T., H.S., M.S., K.F., T.W., and M.N. approved the final version of the manuscript.

REFERENCES

1. **Akizawa T, Nangaku M, Yamaguchi T, Arai M, Koretomo R, Maeda K, Miyazawa Y, Hirakata H.** Enarodustat, Conversion and maintenance therapy for anemia in hemodialysis patients: a randomized, placebo-controlled phase 2b trial followed by long-term trial. *Nephron* 143: 77–85, 2019. doi:10.1159/000500487.
2. **Akizawa T, Nangaku M, Yamaguchi T, Arai M, Koretomo R, Matsui A, Hirakata H.** A placebo-controlled, randomized trial of enarodustat in patients with chronic kidney disease followed by long-term trial. *Am J Nephrol* 49: 165–174, 2019. doi:10.1159/000496929.
3. **Amann K, Rychlík I, Miltenberger-Milteny G, Ritz E.** Left ventricular hypertrophy in renal failure. *Kidney Int Suppl* 68: S78–S85, 1998. doi:10.1046/j.1523-1755.1998.06818.x.
4. **Berl T, Henrich W.** Kidney-heart interactions: epidemiology, pathogenesis, and treatment. *Clin J Am Soc Nephrol* 1: 8–18, 2006. doi:10.2215/CJN.00730805.
5. **Bernhardt WM, Câmpean V, Kany S, Jürgensen JS, Weidemann A, Warnecke C, Arend M, Klaus S, Günzler V, Amann K, Willam C, Wiesener MS, Eckardt KU.** Preconditional activation of hypoxia-inducible factors ameliorates ischemic acute renal failure. *J Am Soc Nephrol* 17: 1970–1978, 2006. doi:10.1681/ASN.2005121302.
6. **Bidani AK, Polichnowski AJ, Loutzenhiser R, Griffin KA.** Renal microvascular dysfunction, hypertension and CKD progression. *Curr Opin Nephrol Hypertens* 22: 1–9, 2013. doi:10.1097/MNH.0b013e32835b36c1.
7. **Bongartz LG, Braam B, Verhaar MC, Cramer MJ, Goldschmeding R, Gaillard CA, Doevendans PA, Joles JA.** Transient nitric oxide reduction induces permanent cardiac systolic dysfunction and worsens kidney damage in rats with chronic kidney disease. *Am J Physiol Regul Integr Comp Physiol* 298: R815–R823, 2010. doi:10.1152/ajpregu.00727.2009.
8. **Chen L, Gong Q, Stice JP, Knowlton AA.** Mitochondrial OPA1, apoptosis, and heart failure. *Cardiovasc Res* 84: 91–99, 2009. doi:10.1093/cvr/cvp181.
9. **Chen RL, Ogunshola OO, Yeoh KK, Jani A, Papadakis M, Nagel S, Schofield CJ, Buchan AM.** HIF prolyl hydroxylase inhibition prior to transient focal cerebral ischaemia is neuroprotective in mice. *J Neurochem* 131: 177–189, 2014. doi:10.1111/jnc.12804.
10. **Flachskampf FA, Biering-Sørensen T, Solomon SD, Duvernoy O, Bjerner T, Smiseth OA.** Cardiac imaging to evaluate left ventricular diastolic function. *JACC Cardiovasc Imaging* 8: 1071–1093, 2015. doi:10.1016/j.jcmg.2015.07.004.
11. **Go AS, Chertow GM, Fan D, McCulloch CE, Hsu CY.** Chronic kidney disease and the risks of death, cardiovascular events, and hospitalization. *N Engl J Med* 351: 1296–1305, 2004. doi:10.1056/NEJMoa041031.
12. **Goel HL, Mercurio AM.** VEGF targets the tumour cell. *Nat Rev Cancer* 13: 871–882, 2013. doi:10.1038/nrc3627.
13. **Habara-Ohkubo A.** Differentiation of beating cardiac muscle cells from a derivative of P19 embryonal carcinoma cells. *Cell Struct Funct* 21: 101–110, 1996. doi:10.1247/csf.21.101.
14. **Ham O, Jin W, Lei L, Huang HH, Tsuji K, Huang M, Roh J, Rosenzweig A, Lu HAJ.** Pathological cardiac remodeling occurs early in

CKD mice from unilateral urinary obstruction, and is attenuated by Enalapril. *Sci Rep* 8: 16087, 2018. doi:10.1038/s41598-018-34216-x.

15. **Hill P, Shukla D, Tran MG, Aragones J, Cook HT, Carmeliet P, Maxwell PH.** Inhibition of hypoxia inducible factor hydroxylases protects against renal ischemia-reperfusion injury. *J Am Soc Nephrol* 19: 39–46, 2008. doi:10.1681/ASN.2006090998.
16. **Hölscher M, Silter M, Krull S, von Ahlen M, Hesse A, Schwartz P, Wielockx B, Breier G, Katschinski DM, Zieseniss A.** Cardiomyocyte-specific prolyl-4-hydroxylase domain 2 knock out protects from acute myocardial ischemic injury. *J Biol Chem* 286: 11185–11194, 2011. doi:10.1074/jbc.M110.186809.
17. **Hyvärinen J, Hassinen IE, Sormunen R, Mäki JM, Kivirikko KI, Koivunen P, Myllyharju J.** Hearts of hypoxia-inducible factor prolyl 4-hydroxylase-2 hypomorphic mice show protection against acute ischemia-reperfusion injury. *J Biol Chem* 285: 13646–13657, 2010. doi:10.1074/jbc.M109.084855.
18. **Kapitsinou PP, Jaffe J, Michael M, Swan CE, Duffy KJ, Erickson-Miller CL, Haase VH.** Preischemic targeting of HIF prolyl hydroxylation inhibits fibrosis associated with acute kidney injury. *Am J Physiol Renal Physiol* 302: F1172–F1179, 2012. doi:10.1152/ajprenal.00667.2011.
19. **Kido M, Du L, Sullivan CC, Li X, Deutsch R, Jamieson SW, Thistlethwaite PA.** Hypoxia-inducible factor 1-alpha reduces infarction and attenuates progression of cardiac dysfunction after myocardial infarction in the mouse. *J Am Coll Cardiol* 46: 2116–2124, 2005. doi:10.1016/j.jacc.2005.08.045.
20. **Levin A, Thompson CR, Ethier J, Carlisle EJ, Tobe S, Mendelssohn D, Burgess E, Jindal K, Barrett B, Singer J, Djurdjev O.** Left ventricular mass index increase in early renal disease: impact of decline in hemoglobin. *Am J Kidney Dis* 34: 125–134, 1999. doi:10.1016/S0272-6386(99)70118-6.
21. **Li X, Cui XX, Chen YJ, Wu TT, Xu H, Yin H, Wu YC.** Therapeutic potential of a prolyl hydroxylase inhibitor FG-4592 for Parkinson's diseases *in vitro* and *in vivo*: regulation of redox biology and mitochondrial function. *Front Aging Neurosci* 10: 121, 2018. doi:10.3389/fnagi.2018.00121.
22. **London GM.** Left ventricular hypertrophy: why does it happen? *Nephrol Dial Transplant* 18, *Suppl* 8: viii: 2–6, 2003. doi:10.1093/ndt/gfg1083.
23. **Morkin E.** Control of cardiac myosin heavy chain gene expression. *Microsc Res Tech* 50: 522–531, 2000. doi:10.1002/1097-0029(20000915)50:6<522:AID-JEMT9>3.0.CO;2-U.
24. **Nangaku M.** Chronic hypoxia and tubulointerstitial injury: a final common pathway to end-stage renal failure. *J Am Soc Nephrol* 17: 17–25, 2006. doi:10.1681/ASN.2005070757.
25. **Natarajan R, Salloum FN, Fisher BJ, Ownby ED, Kukreja RC, Fowler AA III.** Activation of hypoxia-inducible factor-1 via prolyl-4 hydoxylase-2 gene silencing attenuates acute inflammatory responses in postischemic myocardium. *Am J Physiol Heart Circ Physiol* 293: H1571–H1580, 2007. doi:10.1152/ajpheart.00291.2007.
26. **Ogoshi Y, Matsui T, Mitani I, Yokota M, Terashita M, Motoda D, Ueyama K, Hotta T, Ito T, Hase Y, Fukui K, Deai K, Yoshiuchi H, Ito S, Abe H.** Discovery of JTZ-951: a HIF prolyl hydroxylase inhibitor for the treatment of renal anemia. *ACS Med Chem Lett* 8: 1320–1325, 2017. doi:10.1021/acsmedchemlett.7b00404.
27. **Olson E, Demopoulos L, Haws TF, Hu E, Fang Z, Mahar KM, Qin P, Lepore J, Bauer TA, Hiatt WR.** Short-term treatment with a novel HIF-prolyl hydroxylase inhibitor (GSK1278863) failed to improve measures of performance in subjects with claudication-limited peripheral artery disease. *Vasc Med* 19: 473–482, 2014. doi:10.1177/1358863X14557151.
28. **Otera H, Mihara K.** Molecular mechanisms and physiologic functions of mitochondrial dynamics. *J Biochem* 149: 241–251, 2011. doi:10.1093/jb/mvr002.
29. **Pisano A, Cerbelli B, Perli E, Pelullo M, Bargelli V, Preziuso C, Mancini M, He L, Bates MG, Lucena JR, Della Monica PL, Familiari G, Petrozza V, Nediani C, Taylor RW, d'Amati G, Giordano C.** Impaired mitochondrial biogenesis is a common feature to myocardial hypertrophy and end-stage ischemic heart failure. *Cardiovasc Pathol* 25: 103–112, 2016. doi:10.1016/j.carpath.2015.09.009.
30. **Portolés J, Torralbo A, Martin P, Rodrigo J, Herrero JA, Barrientos A.** Cardiovascular effects of recombinant human erythropoietin in predialysis patients. *Am J Kidney Dis* 29: 541–548, 1997. doi:10.1016/S0272-6386(97)90335-8.
31. **Ronco C, Haapio M, House AA, Anavekar N, Bellomo R.** Cardiorenal syndrome. *J Am Coll Cardiol* 52: 1527–1539, 2008. doi:10.1016/j.jacc.2008.07.051.
32. **Rosenkranz S.** TGF-beta1 and angiotensin networking in cardiac remodeling. *Cardiovasc Res* 63: 423–432, 2004. doi:10.1016/j.cardiores.2004.04.030.
33. **Rowe GC, Jiang A, Arany Z.** PGC-1 coactivators in cardiac development and disease. *Circ Res* 107: 825–838, 2010. doi:10.1161/CIRCRESAHA.110.223818.
34. **Sano M, Minamino T, Toko H, Miyauchi H, Orimo M, Qin Y, Akazawa H, Tateno K, Kayama Y, Harada M, Shimizu I, Asahara T, Hamada H, Tomita S, Molkentin JD, Zou Y, Komuro I.** p53-induced inhibition of Hif-1 causes cardiac dysfunction during pressure overload. *Nature* 446: 444–448, 2007. doi:10.1038/nature05602.
35. **Schefold JC, Filippatos G, Hasenfuss G, Anker SD, von Haehling S.** Heart failure and kidney dysfunction: epidemiology, mechanisms and management. *Nat Rev Nephrol* 12: 610–623, 2016. doi:10.1038/nrneph.2016.113.
36. **Schönenberger MJ, Kovacs WJ.** Hypoxia signaling pathways: modulators of oxygen-related organelles. *Front Cell Dev Biol* 3: 42, 2015. doi:10.3389/fcell.2015.00042.
37. **Semenza GL.** Hypoxia-inducible factor 1 and cardiovascular disease. *Annu Rev Physiol* 76: 39–56, 2014. doi:10.1146/annurev-physiol-021113-170322.
38. **Semenza GL.** Oxygen sensing, homeostasis, and disease. *N Engl J Med* 365: 537–547, 2011. doi:10.1056/NEJMra1011165.
39. **Siedlecki AM, Jin X, Muslin AJ.** Uremic cardiac hypertrophy is reversed by rapamycin but not by lowering of blood pressure. *Kidney Int* 75: 800–808, 2009. doi:10.1038/ki.2008.690.
40. **Smith K, Semple D, Aksentijevic D, Bhandari S, Seymour AM.** Functional and metabolic adaptation in uraemic cardiomyopathy. *Front Biosci (Elite Ed)* 2: 1492–1501, 2010. doi:10.2741/e208.
41. **Song YR, You SJ, Lee YM, Chin HJ, Chae DW, Oh YK, Joo KW, Han JS, Na KY.** Activation of hypoxia-inducible factor attenuates renal injury in rat remnant kidney. *Nephrol Dial Transplant* 25: 77–85, 2010. doi:10.1093/ndt/gfp454.
42. **Suen DF, Norris KL, Youle RJ.** Mitochondrial dynamics and apoptosis. *Genes Dev* 22: 1577–1590, 2008. doi:10.1101/gad.1658508.
43. **Sugahara M, Tanaka T, Nangaku M.** Prolyl hydroxylase domain inhibitors as a novel therapeutic approach against anemia in chronic kidney disease. *Kidney Int* 92: 306–312, 2017. doi:10.1016/j.kint.2017.02.035.
44. **Szabo AJ, Muller V, Chen GF, Samsell LJ, Erdely A, Baylis C.** Nephron number determines susceptibility to renal mass reduction-induced CKD in Lewis and Fisher 344 rats: implications for development of experimentally induced chronic allograft nephropathy. *Nephrol Dial Transplant* 23: 2492–2495, 2008. doi:10.1093/ndt/gfn112.
45. **Tanaka T, Eckardt KU.** HIF activation against CVD in CKD: novel treatment opportunities. *Semin Nephrol* 38: 267–276, 2018. doi:10.1016/j.semnephrol.2018.02.006.
46. **Tanaka T, Kojima I, Ohse T, Ingelfinger JR, Adler S, Fujita T, Nangaku M.** Cobalt promotes angiogenesis via hypoxia-inducible factor and protects tubulointerstitium in the remnant kidney model. *Lab Invest* 85: 1292–1307, 2005. doi:10.1038/labinvest.3700328.
47. **Tanaka T, Yamaguchi J, Higashijima Y, Nangaku M.** Indoxyl sulfate signals for rapid mRNA stabilization of Cbp/p300-interacting transactivator with Glu/Asp-rich carboxy-terminal domain 2 (CITED2) and suppresses the expression of hypoxia-inducible genes in experimental CKD and uremia. *FASEB J* 27: 4059–4075, 2013. doi:10.1096/fj.13-231837.
48. **Tang Y, Mi C, Liu J, Gao F, Long J.** Compromised mitochondrial remodeling in compensatory hypertrophied myocardium of spontaneously hypertensive rat. *Cardiovasc Pathol* 23: 101–106, 2014. doi:10.1016/j.carpath.2013.11.002.
49. **Tsushima K, Osawa T, Yanai H, Nakajima A, Takaoka A, Manabe I, Ohba Y, Imai Y, Taniguchi T, Nagai R.** IRF3 regulates cardiac fibrosis but not hypertrophy in mice during angiotensin II-induced hypertension. *FASEB J* 25: 1531–1543, 2011. doi:10.1096/fj.10-174615.
50. **Vogler M, Zieseniss A, Hesse AR, Levent E, Tiburcy M, Heinze E, Burzlaff N, Schley G, Eckardt KU, Willam C, Katschinski DM.** Pre- and post-conditional inhibition of prolyl-4-hydroxylase domain enzymes protects the heart from an ischemic insult. *Pflugers Arch* 467: 2141–2149, 2015. doi:10.1007/s00424-014-1667-z.
51. **Wu J, Chen P, Li Y, Ardell C, Der T, Shohet R, Chen M, Wright GL.** HIF-1α in heart: protective mechanisms. *Am J Physiol Heart Circ Physiol* 305: H821–H828, 2013. doi:10.1152/ajpheart.00140.2013.

52. **Wu Z, Puigserver P, Andersson U, Zhang C, Adelmant G, Mootha V, Troy A, Cinti S, Lowell B, Scarpulla RC, Spiegelman BM.** Mechanisms controlling mitochondrial biogenesis and respiration through the thermogenic coactivator PGC-1. *Cell* 98: 115–124, 1999. doi:10.1016/S0092-8674(00)80611-X.
53. **Yu X, Fang Y, Liu H, Zhu J, Zou J, Xu X, Jiang S, Ding X.** The balance of beneficial and deleterious effects of hypoxia-inducible factor activation by prolyl hydroxylase inhibitor in rat remnant kidney depends on the timing of administration. *Nephrol Dial Transplant* 27: 3110–3119, 2012. doi:10.1093/ndt/gfr754.
54. **Zhu Q, Wang Z, Xia M, Li PL, Van Tassell BW, Abbate A, Dhaduk R, Li N.** Silencing of hypoxia-inducible factor-1α gene attenuated angiotensin II-induced renal injury in Sprague-Dawley rats. *Hypertension* 58: 657–664, 2011. doi:10.1161/HYPERTENSIONAHA.111.177626.